Addressing non-stationary shear wave statics in the rayparameter domain

Raul Cova, David Henley and Kris Innanen

ABSTRACT

When velocity contrasts at the base of the near-surface layer are small, or when it shows some degree of structural complexity, delay times of wavefronts transmitted through this layer may become raypath dependent. Due to the low velocity of S-waves this dependency is translated into significant non-stationary delays. In order to remove this effect we transform the data to a domain in which amplitudes are a function of the raypath angle. Processing the statics in the radial trace (RT), Snell trace (ST) and τ-p domain achieve this goal, but with different degrees of accuracy. Since the first two domains involve only a very simple remapping of the amplitude from the original x-t domain they are free of the numerical problems experienced with the τ-p transform. However, the RT and ST transformations require that some assumptions about the subsurface velocity model must be made. On the other hand, the τ-p transform automatically scans the data in order to capture the rayparameter values that were actually recorded. The surface correction of synthetic data in a depth-varying velocity medium showed that the solutions obtained in the ST and τ-p domain are very similar, while common offset and RT solutions still show some unresolved problems. Further analysis was performed using real data from the Hussar experiment. Results showed that the τ-p solution provided a better stacking power in the deeper part of the section. In the shallow part the RT and ST solution seem to have better resolution. Further work is needed to reduce the artifacts present in the τ-p transformation. Trying a high resolution τ-p transform will be the next step in this research.

INTRODUCTION

In treating multicomponent seismic data on land and on the ocean bottom, proper management of the complex near surface is a critical step. This is increasingly true as acquisition of broadband, wide-azimuth seismic data becomes the norm, and as the potential for full waveform inversion of land data becomes real, requiring both modelling of waves in the near surface and accurate accounting for surface wave modes. We seek an improvement in the converted wave statics solution not only as measured by our standard metrics, but also in the sense of physical completeness.

Within the context of seismic reflections, static time delays are the product of low-velocity sediments present near the surface. Changes in the velocity and thickness of these sediments introduce additional delays in the reflection traveltimes that may disturb the actual structure and alignment of the subsurface reflections. This problem is magnified in the case of converted-wave data due to the very low velocities of shear waves. In addition, the shear-wave velocity contrast at the base of the near surface may not be large enough to support the vertical raypath assumption that is conventionally used in the computation of static corrections. Cova et al. (2013) show how even if the velocity contrast at the base of the near surface is large, the presence of dip may cause raypath-dependent delays that may differ significantly from the vertical traveltimes in the near surface.
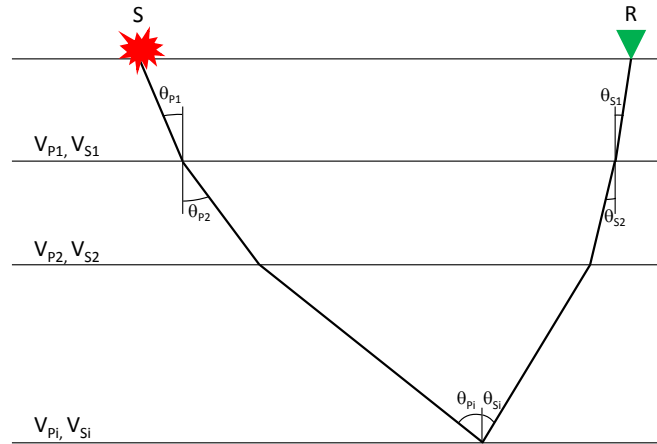
FIG. 1. Schematic representation of a PS-wave raypath. Despite the asymmetry in the raypath the rayparameter value $p = \sin(\theta_i/V_i)$ is constant for a horizontally layered medium.

Henley (2012, 2014) showed how statics can be solved in the radial-trace domain by using the radial-trace (RT) and Snell-trace (ST) transforms. Both approaches solve the problem of raypath-dependent statics by moving the data to a domain where amplitudes are a function of raypath angle. However, both transforms make assumptions about the velocities controlling the changes in the rayparameter values. While the RT transform remaps amplitudes assuming an underlying constant velocity model the ST transform assumes a smooth velocity change with depth. Here we propose using the τ-p transform as a more complete way for moving the data to the rayparameter domain. In this study we will use the same interferometric approach presented by Henley (2012) but considering the τ-p transform as an alternative to move the data to a raypath-consistent framework. Results on synthetic and real data from the Hussar experiment will be analyzed to show the pros and cons of computing shear-wave statics corrections in the τ-p domain.

MOVING THE DATA TO A RAYPATH-CONSISTENT FRAMEWORK

Data analysis in the rayparameter domain

According to Snell's law the rayparameter p is a constant quantity when the propagation of the wavefield occurs in a horizontally layered media. This criterion of conservation of the horizontal slowness ($p = dt/dx$) can be applied to the propagation of converted waves. Hence, equation 1 must hold for the PS raypath depicted in Figure 1

$$p = \frac{\sin(\theta_{Pi})}{V_{Pi}} = \frac{\sin(\theta_{Si})}{V_{Si}}, \tag{1}$$

where V_{Pi} and V_{Si} are the P- and the S-wave velocities in the $i - th$ layer, θ_P and θ_S are the P- and S-wave propagation angles. This expression allows us to characterize the full raypath of a converted-wave by using a single rayparameter value despite the difference in velocity between the P- and S-wave legs.

The rayparameter "p" when measured from data recorded with surface arrays is related to the emerging angle of the wavefield at the surface (Tatham (1989)). This feature makes the rayparameter domain a good candidate for understanding near surface effects. To trans-
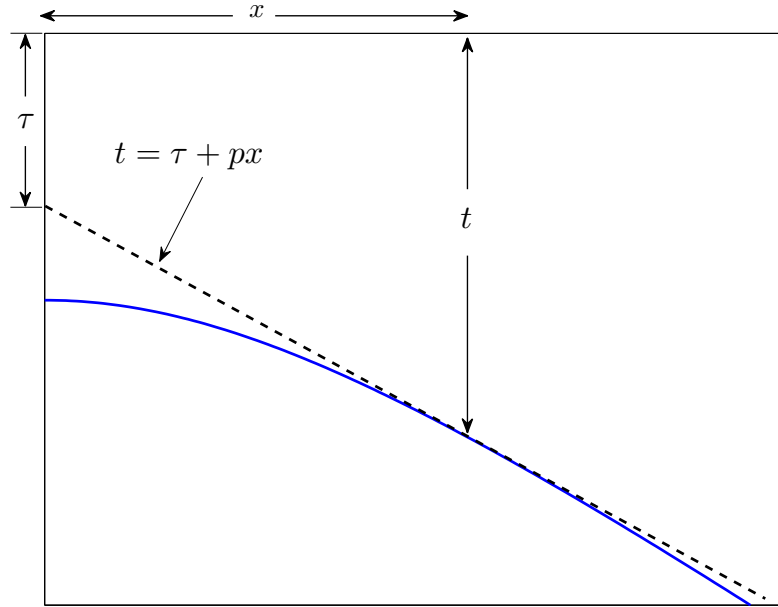
FIG. 2. Representation of the τ-p transform. Amplitudes along the line $t = \tau + px$ are stacked and mapped into the new domain.

form the data to the rayparameter domain the "slant-stack" or τ-p transforms can be used (Claerbout (1975); Stoffa (1989)). The transformation is achieved by stacking data along straight lines within a given range of slopes (p) and intercept times (τ). Equation 2 shows the integral definition of the τ-p transform acting on the x-t domain,

$$\tilde{u}(\tau, p) = \int_{-\infty}^{\infty} u(\tau + px, x)dx. \tag{2}$$

Since seismic reflection data exhibit hyperbolic moveout, the τ-p transform amounts to scanning for all the possible tangents that define such hyperbolae. The "scanning" character of the transform relieves it from needing any a-priori knowledge of the velocity model of the subsurface.

The inverse τ-p transform is defined as,

$$u(t, x) = -\frac{1}{2\pi} \int_{-\infty}^{\infty} \tilde{u}^{\dagger}(t - px, p)dp. \tag{3}$$

where $\tilde{u}^{\dagger}(\tau, p)$ is the derivative of the Hilbert transform of $\tilde{u}(\tau, p)$. The transform pair defined in equations 2 and 3 is often used for plane wave decomposition since $\tilde{u}(\tau, p)$ represents the plane-wave response of a laterally homogeneous model to a line source. Hence, it very useful for studying two dimensional wave propagation in a model with variation in one-dimension (Chapman, 1978).

Figure 2 shows a schematic of a seismic gather in the x-t domain and the τ-p transform operation. It is important to note that due to the limited aperture and limited bandwidth of the seismic data the transformation produces some artifacts. This feature and the numerical incompleteness of its inverse transform are the weak points of the τ-p transform.
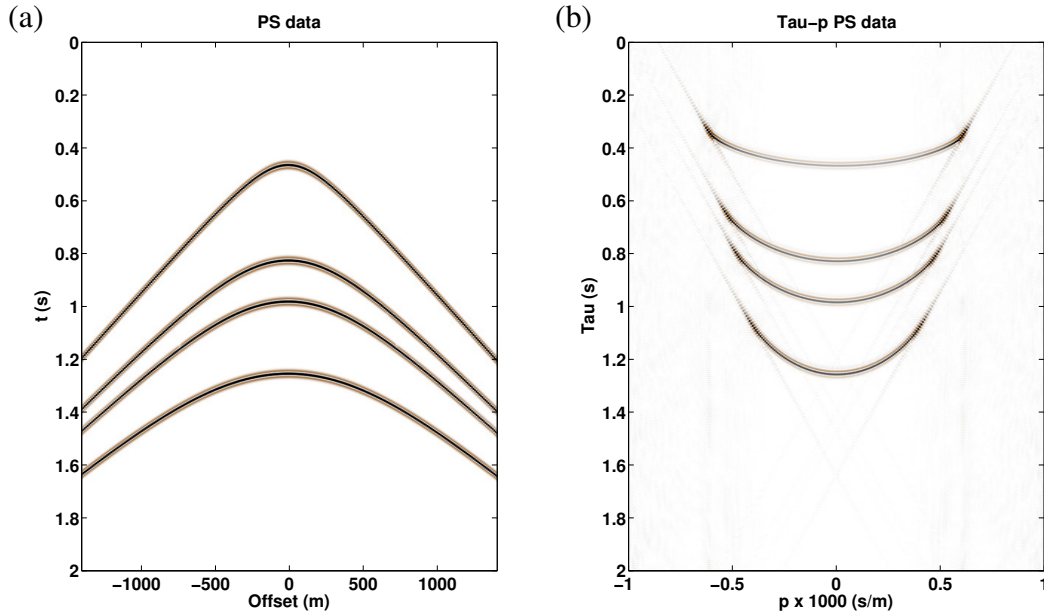
FIG. 3. (a) Synthetic shot gather. (b) τ-p transformation.

The radial trace transform

The radial trace transform consists of a deformation of the time-space domain into a radial domain via the expression,

$$u'(t,r) = u(t, rt) \qquad (4)$$

where r is the radial-trace parameter defined as $r = x/t$ ((Claerbout, 1985)).

Since the RT-transform involves just a remapping of the amplitudes values it can be rewritten using the sifting property as,

$$u'(t,r) = \int_{-\infty}^{\infty} u(t,x)\delta(x - rt)dx \qquad (5)$$

From equation 5 we can see that the effect of the RT-transform is that of resampling the amplitudes recorded in the x-t domain along lines of constant slope. All the amplitudes gathered along each one of the lines form a new radial trace.

Figure 4 shows the geometrical construction of the RT-transform. There we can note that the RT-transform seems to be related to the τ-p transform in the following way: First, the RT transform operates along lines that intersect the coordinate system at a fixed location. Having a constant intersection with the time axis is equivalent to having a fixed τ value (usually 0, in most RT applications) in the τ-p transform. Secondly, the slope of the trajectories in the RT-transform is $1/r$ while in the τ-p transform is p then, for a constant velocity medium the radial trace parameter can be seen as the reciprocal of the rayparameter. Lastly, since the RT-transform involves just a remapping of the amplitudes as defined by equation 4, amplitudes never get stacked. Thus, the RT-transform can be seen as the
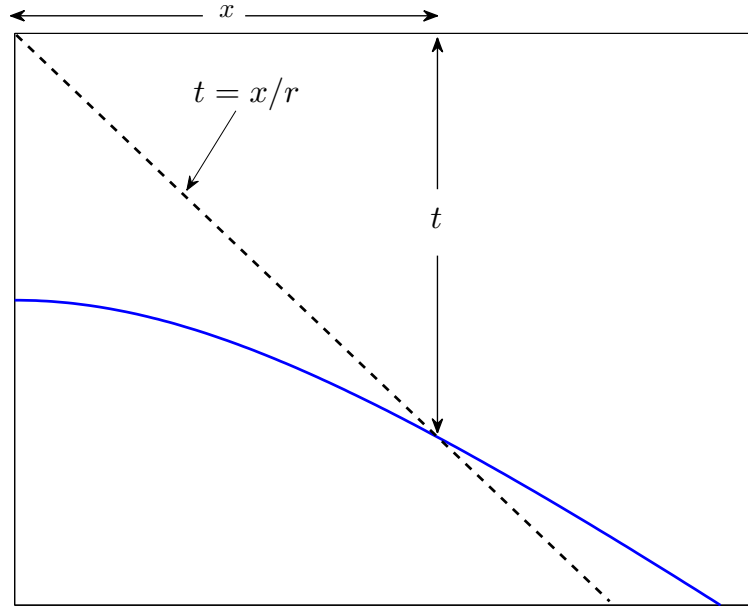
FIG. 4. Representation of the RT transform. Amplitudes along the line $t = x/r$ are gathered to from a new trace in the RT domain.

gathering of all the data needed to compute the amplitudes along a constant τ value in the τ-p domain. To show this let us evaluate equation 2 for $\tau = 0$ and rewrite it using the sifting property of the delta function,

$$\tilde{u}(0, p) = \int_{-\infty}^{\infty} u(px, x)dx, \tag{6}$$

$$= \int_{-\infty}^{\infty} \int_{-\infty}^{\infty} u(t, x)\delta(t - px)dtdx. \tag{7}$$

Using the scaling property of the delta function and changing the order of the terms inside of it we get,

$$\tilde{u}(0, p) = \frac{1}{|p|} \int_{-\infty}^{\infty} \int_{-\infty}^{\infty} u(t, x)\delta\left(x - \frac{t}{p}\right) dtdx, \tag{8}$$

$$= |r| \int_{-\infty}^{\infty} \int_{-\infty}^{\infty} u(t, x)\delta\left(x - rt\right) dtdx, \tag{9}$$

$$= |r| \int_{-\infty}^{\infty} u(t, rt)dt, \tag{10}$$

$$= |r| \int_{-\infty}^{\infty} u'(t, r)dt \tag{11}$$

Equation 11 shows that a radial-trace gather contains all the amplitudes to be stacked for computing the data at a constant τ value in a τ-p gather. To complete the τ-p construction

we will need to compute additional RT gathers where the time-axis intercept assumes each possible value in succession, from 0 to the maximum traveltime. Then, gathering all the traces with the same $1/r$ value, but associated with each of the different intercepts, and stacking them, will provide a trace equivalent to a constant p trace in the τ-p domain.

Despite the simplicity and cheap computational cost of the RT transform, it may not be appropriate for our current purposes when strong velocity changes are present in the data. In this case a transform able to gather amplitudes along nonlinear trajectories may be needed. Figure 5 shows an example of a synthetic gather and its RT-transform. There, it is possible to compare the straight line trajectories used for the RT-transform to gather the amplitude values versus the curved trajectories used in the Snell trace transform. The latter will be described in the next section.

The Snell trace transform

The Snell trace transform can be seen as a generalization of the RT-transform for a flat-layered media with depth varying velocities (Ottolini, 1982). In contrast with the RT transform, The ST transform gathers the amplitudes along curved trajectories in the x-t space. The most important feature is that those trajectories are intended to follow Snell's law. In so doing the ST transform attempts to remap each event so that projected rays follow the velocity changes in the subsurface.

The moveout of reflection events can be approximated by the equation,

$$t = \left(t_0^2 + \frac{x^2}{v_{rms}(t)^2} \right)^{1/2} \tag{12}$$

Following the definition of the rayparameter,

$$p = \frac{dt}{dx} = \frac{1}{2} \left(t_0^2 + \frac{x^2}{v_{rms}(t)^2} \right)^{-1/2} \frac{2x}{v_{rms}(t)^2} \tag{13}$$

$$= \frac{x}{v_{rms}(t)^2 t} \tag{14}$$

By following equation 14 the Snell trace transform tries to extract from the x-t domain the amplitudes that were recorded with the same rayparameter value. If the true velocity model is unknown the sampling trajectories can be updated by assuming a constant linear increment as proposed by Henley (2000). In figure 5 we can see the curved trajectories used in the ST transform and the resulting gathers.

Although more accommodating of velocity variations than the RT transform, the ST transform still needs some a priori information about the velocity model in order to properly gather amplitudes recorded with the same rayparameter value. Its strength is its very simple inversion and very cheap computational cost.

In the following sections application of τ-p, RT and ST transforms over synthetic and

real data will be performed in order to compare the performance of each of them in the solution of raypath dependent statics.
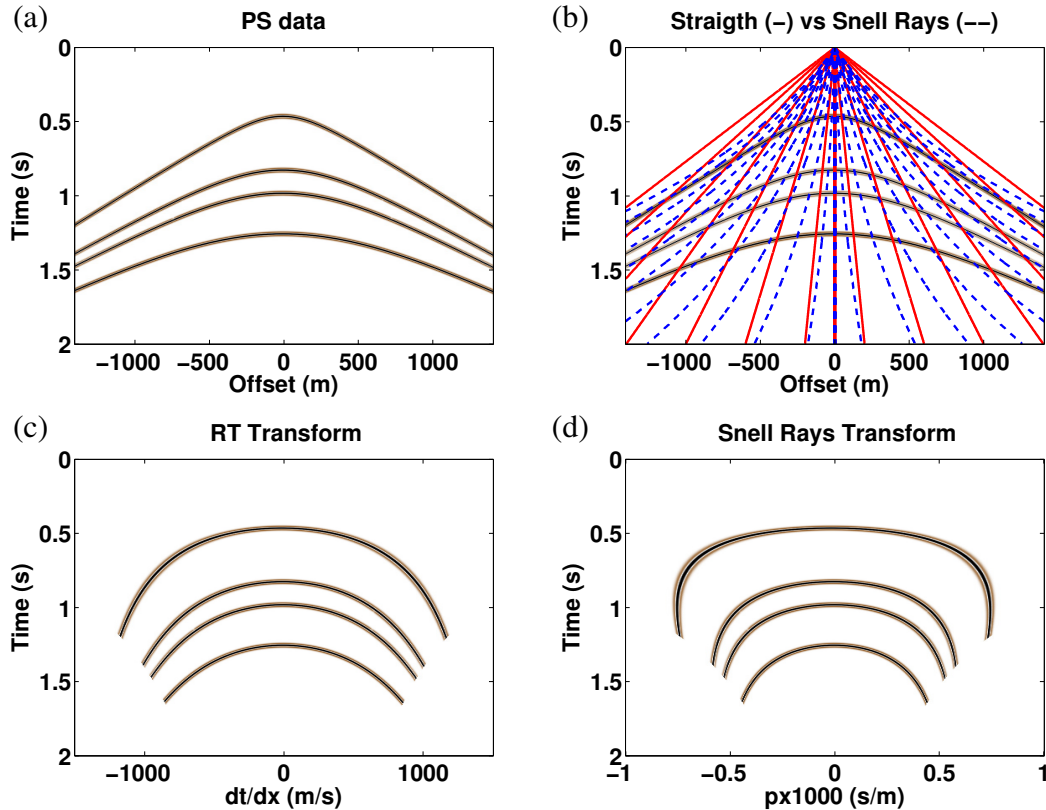

FIG. 5. (a) Synthetic shot gather. (b) RT and ST mapping trajectories. (c) Input data transformed to the RT domain. (d) Input data transformed to the ST domain.

DATA PROCESSING

Synthetic data analysis

Figure 6 shows the velocity model used to compute converted-wave synthetic traces via ray-tracing. The low velocity layer (LVL) at the top shows thicknesses ranging between 20m and 100m and has S-wave velocity of 500 m/s. No P-wave velocity contrast was included between the LVL and the underlying layer in order to bypass P-wave statics. Both the S-wave and P-wave velocities increase monotonically with depth in order to study the effect of these changes on each one of the transforms explained above.

Figure 7 shows the raw ACP stack before applying any correction. In this section the effect of the S-wave statics is very clear, the events are deformed and the stacking power is decreasing with depth.

To understand the stationarity of the S-wave delays produced by the LVL we gather the data into receiver gathers and applied the RT, ST, and τ-p transforms. Figure 8 shows trace panels where data with a common parameter for all the receiver locations are displayed. For example, in the common-offset panel all the traces recorded with an offset of 1500m
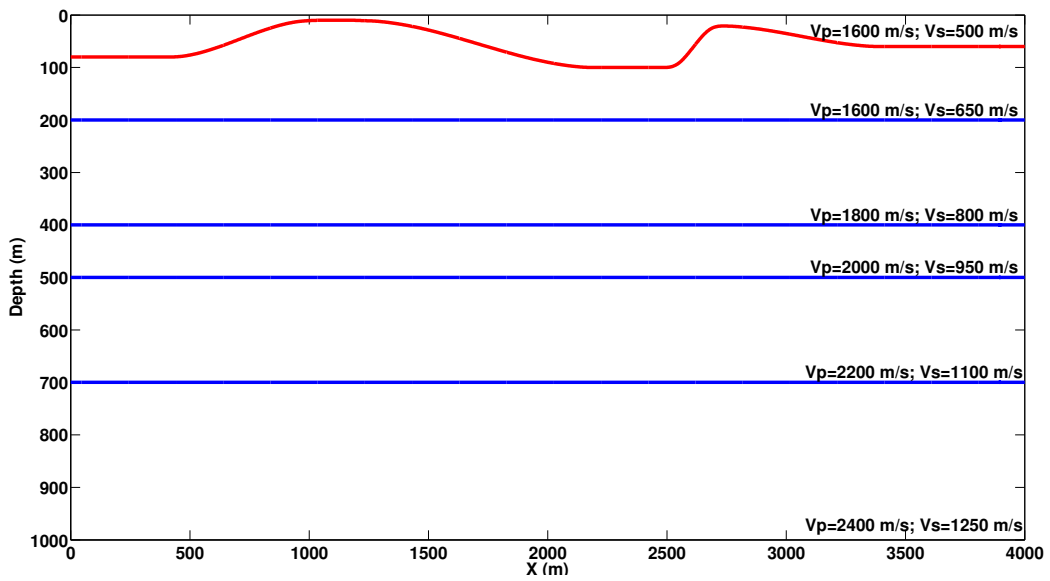
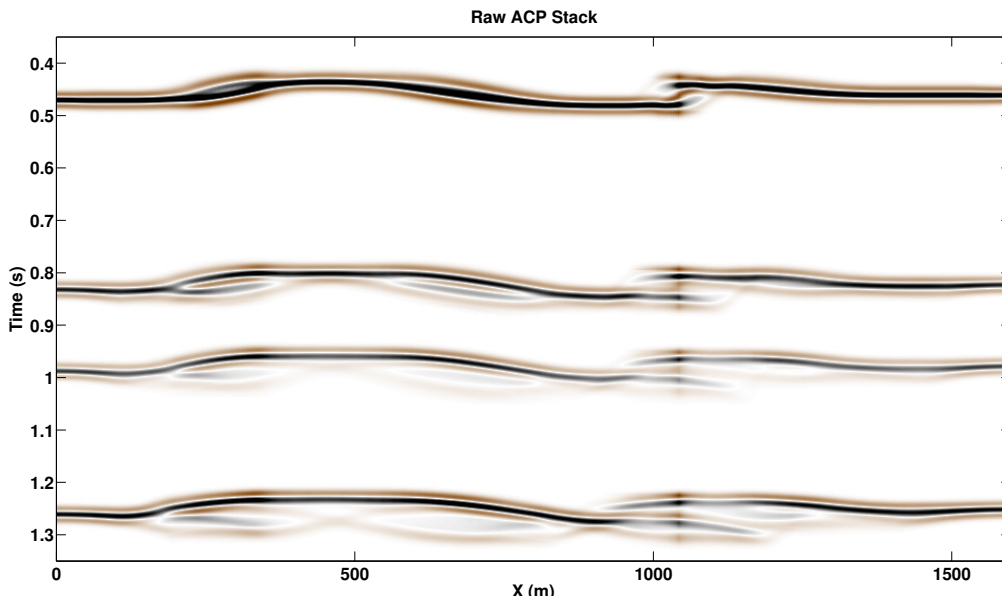FIG. 6. Velocity model used for computing synthetic data.
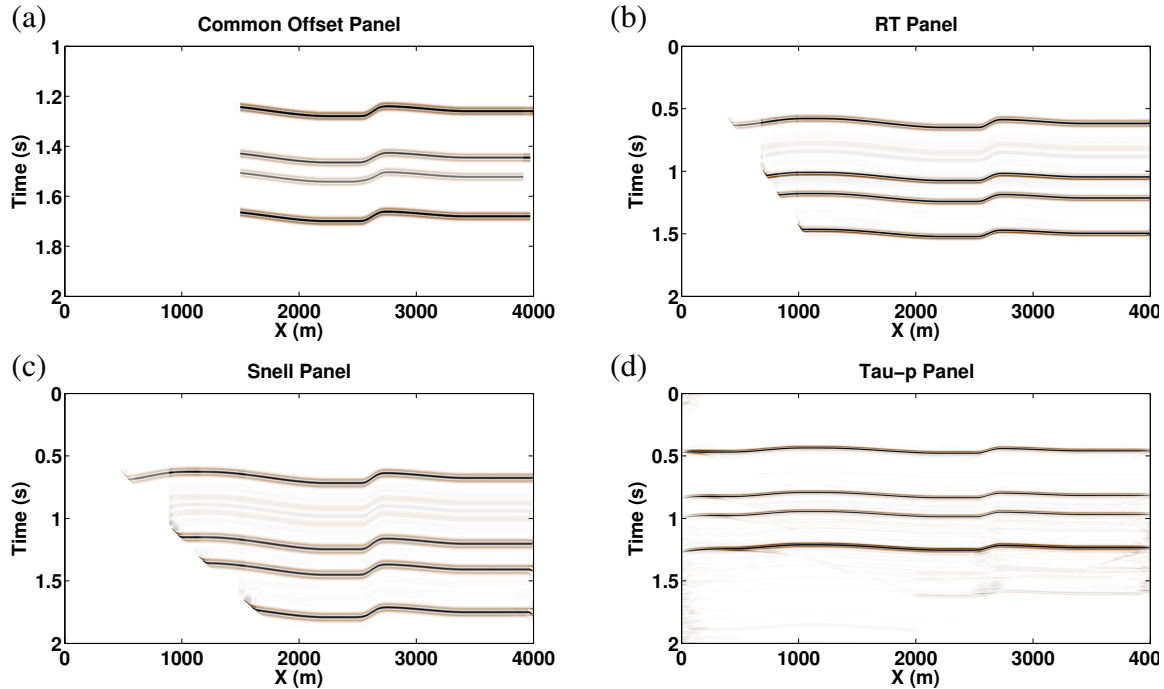

FIG. 7. ACP stack before static corrections.

FIG. 8. Raw data gathered in different domains. (a) Common offset domain. (b) Radial trace domain. (c) Snell trace domain. (d) τ-p domain.

at each receiver location are extracted and plotted according to their location. The other three panels follow the same concept but select the samples according to the parameter that controls each one of the transforms.

To test each one of these domains for stationarity we picked the first event and flattened the data around that event. If the deformations produced by the near surface are of the same magnitude for all the events, then removing the deformation from one of them should correct the deformations on the rest of the reflectors. Figure 9 shows the result of this test. There, it is possible to see how, after flattening the shallow event, there is still a residual deformation on the common-offset, RT and ST panels, particularly around x = 2600m. Only in the τ-p panel the non-stationary character of the statics was fully compensated. In other words, the τ-p transform was able to move the data to a fully stationary condition.

Finally, figure 10 shows the resulting ACP stacks after removing the static effect in each domain. The result in the common-offset domain shows unsolved static problems for the four events, specifically around x=1100m. This problem is likely the result of using the picks of a single common-offset panel to remove the statics from all the dataset. The R-T transform produces high quality statics correction in the three first events. However, for the deepest event the wavelet seems deformed (figure 11). This may be a result of stacking wavelets that are not properly aligned, leading to a decrease of the seismic resolution. The stacks after removing the statics in the Snell-ray and τ-p domain are very similar. There are very small differences in the coherence of the deepest event where the τ-p solution seems to have worked slightly better. However, this result also shows small artifacts in the shallowest part of the section. The Snell-ray transform, although being a "cleaner" solution,
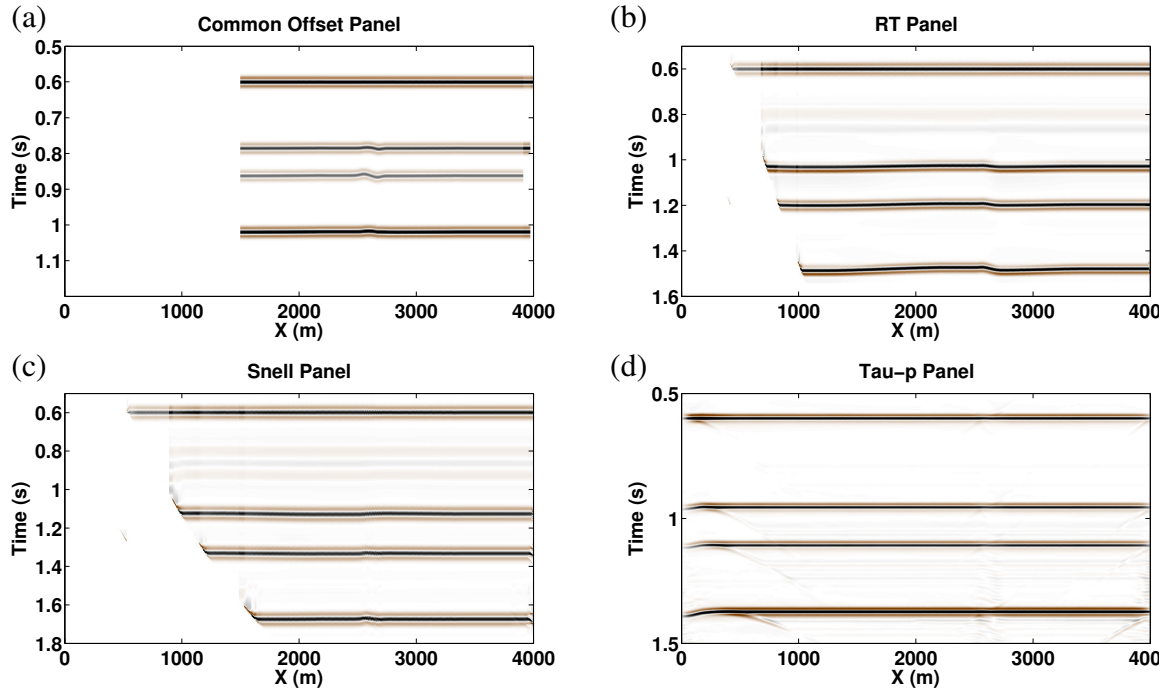
FIG. 9. Results after flattening the data with respect to the shallowest event. (a) Common offset domain. (b) Radial trace domain. (c) Snell trace domain. (d) τ-p domain.

requires some knowledge or assumptions about the velocities in the subsurface.

Processing the Hussar data

Data from the Hussar experiment were processed in order to further compare the performance of the different raypath domains. Details about the acquisition of this data can be found in Margrave et al. (2011).

The interferometric approach used to solve the statics is very similar to the one introduced by Henley (2012). Figure 12 shows the processing workflow used in this research. The general idea is to retrieve the delay times caused by the near surface by cross correlating the raw data with a set of pilot traces. One difference with the work of Henley (2012) is that transformation to the rayparameter domain is done without applying a NMO correction. On this way any residual NMO present in the data is preserved and anisotropic analysis can be performed later. Also, here we introduce the τ-p domain as an option for moving the data to a raypath consistent framework.

Figure 13 shows a raw shot gather. Static problems are evident between the offsets 1500m and 2000m. The event at 1.6s is being pulled down due to low velocities in the near surface.

The same shot gather after applying raypath-consistent static corrections is shown in Figures 14 to 16. There we can see the output after processing the statics in the RT, ST and τ-p domain respectively. The first two effectively removed the pull down of the event at
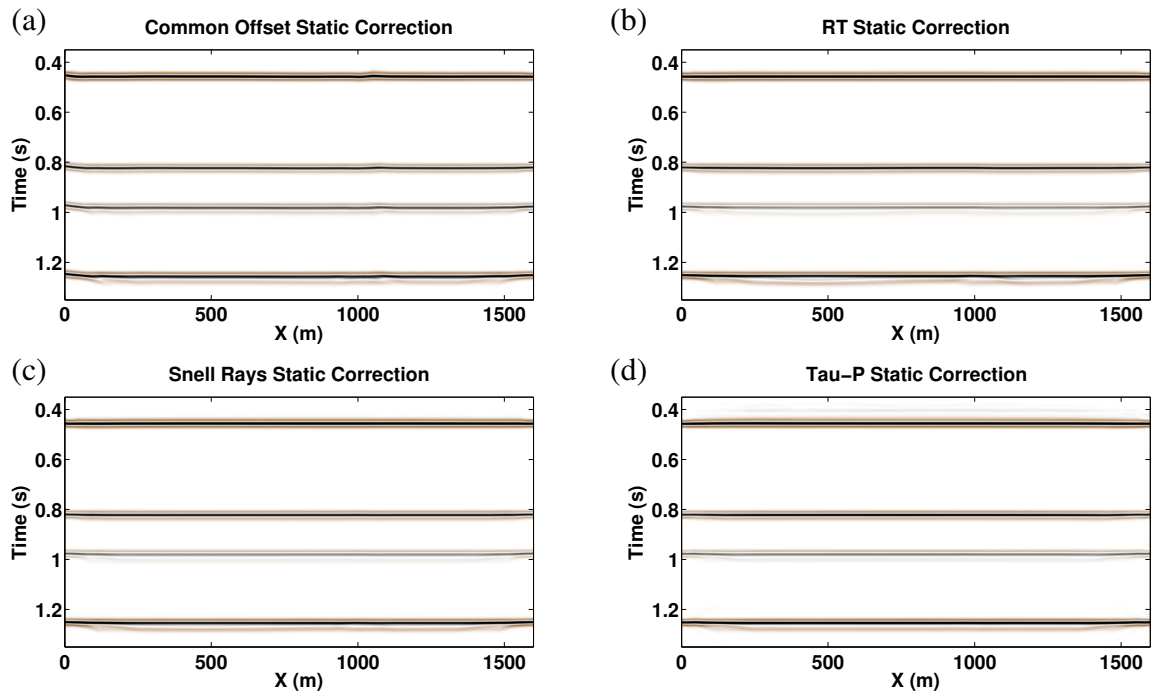
FIG. 10. ACP stacks after removing the statics in each raypath sensitive domain. (a) Common offset domain. (b) Radial trace domain. (c) Snell trace domain. (d) τ-p domain.
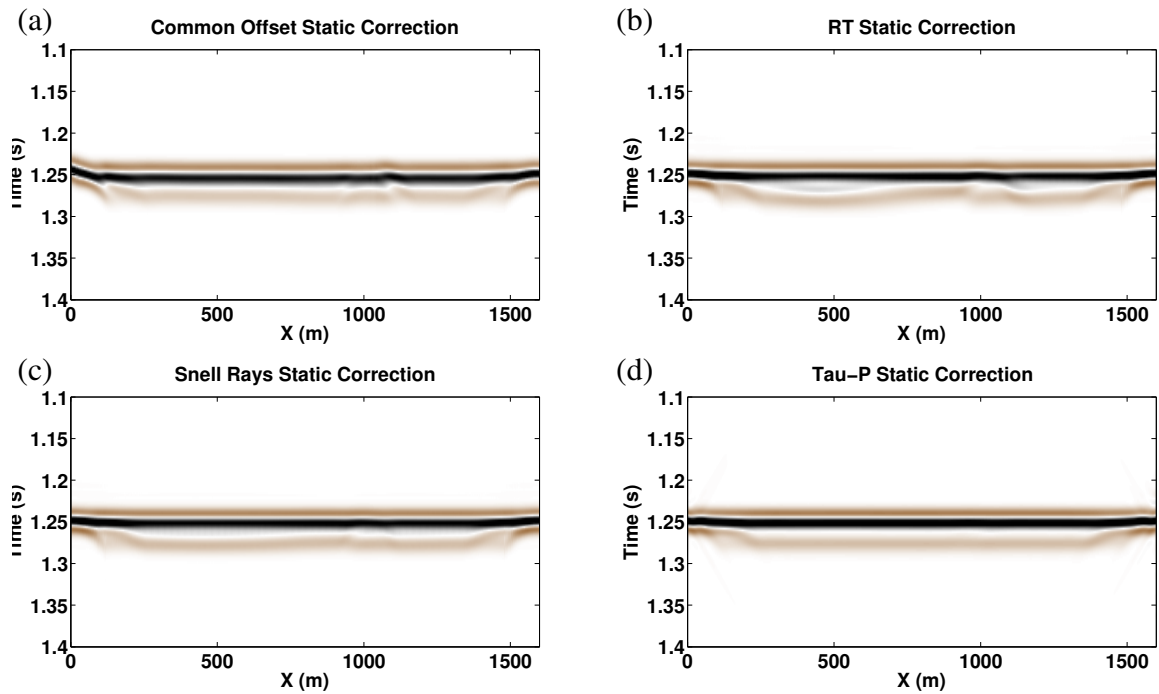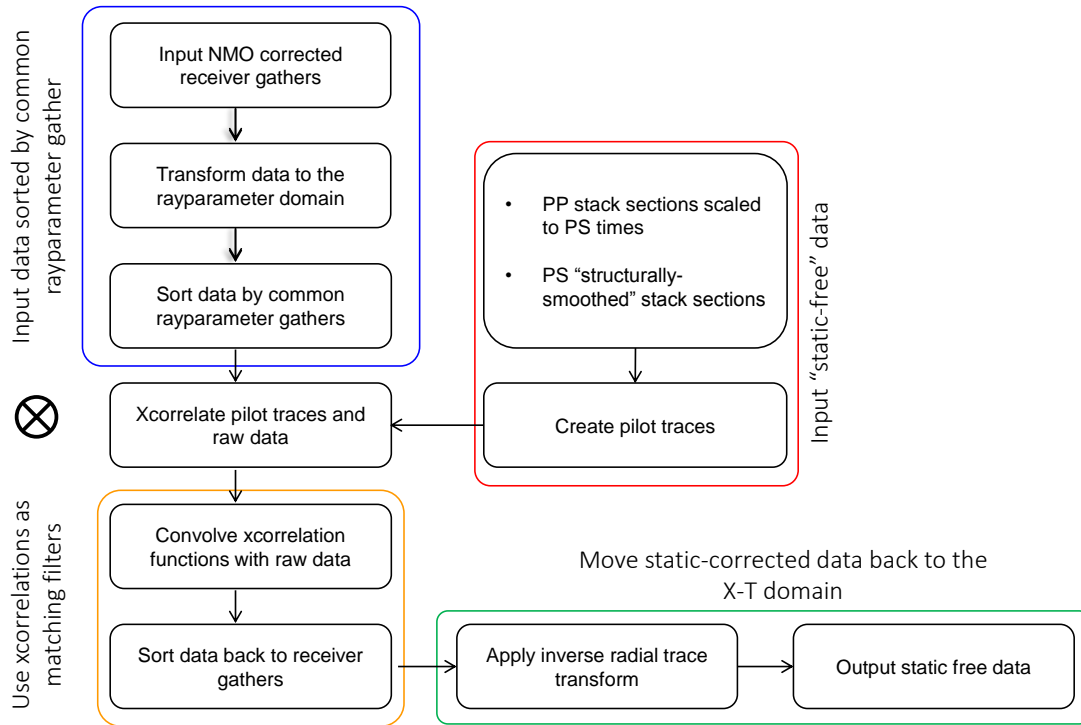
FIG. 11. Zoom around the deep reflector after removing the statics in each raypath sensitive domain. (a) Common offset domain. (b) Radial trace domain. (c) Snell trace domain. (d) τ-p domain.

Input data sorted by common rayparameter gather

Input NMO corrected receiver gathers

Transform data to the rayparameter domain

Sort data by common rayparameter gathers

Input "static-free" data

- PP stack sections scaled to PS times

- PS "structurally-smoothed" stack sections

Xcorrelate pilot traces and raw data

Create pilot traces

Use xcorrelations as matching filters

Convolve xcorrelation functions with raw data

Sort data back to receiver gathers

Move static-corrected data back to the X-T domain

Apply inverse radial trace transform

Output static free data

FIG. 12. Interferometric static correction work flow.
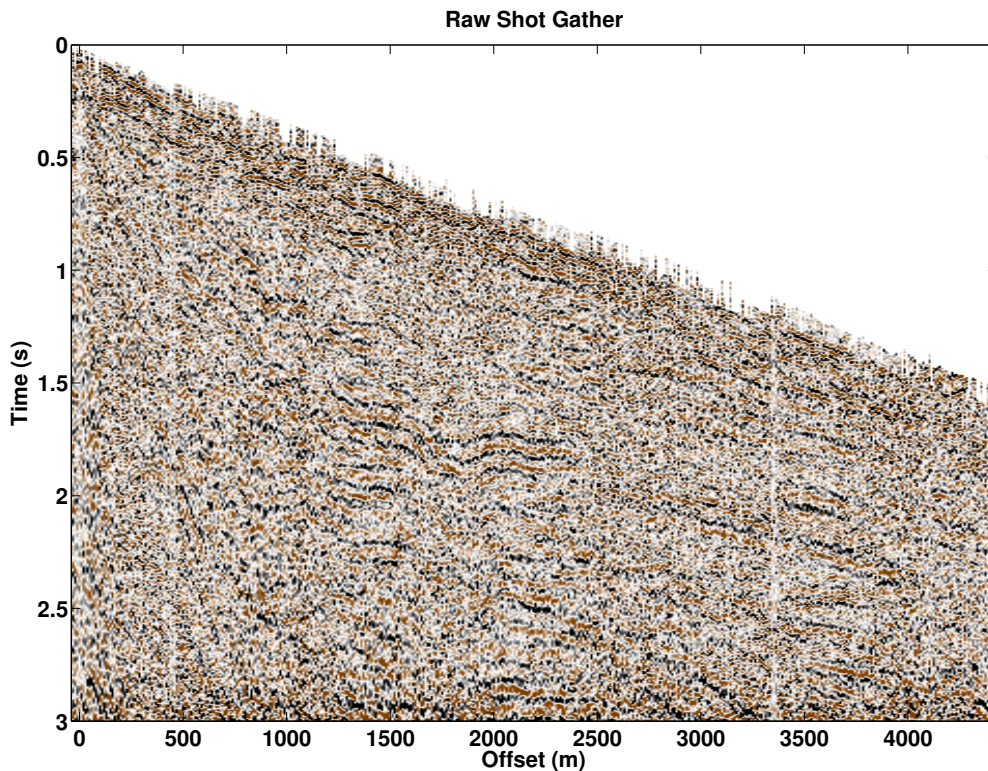
Raw Shot Gather

FIG. 13. Radial component shot gather from the Hussar experiment without static corrections.
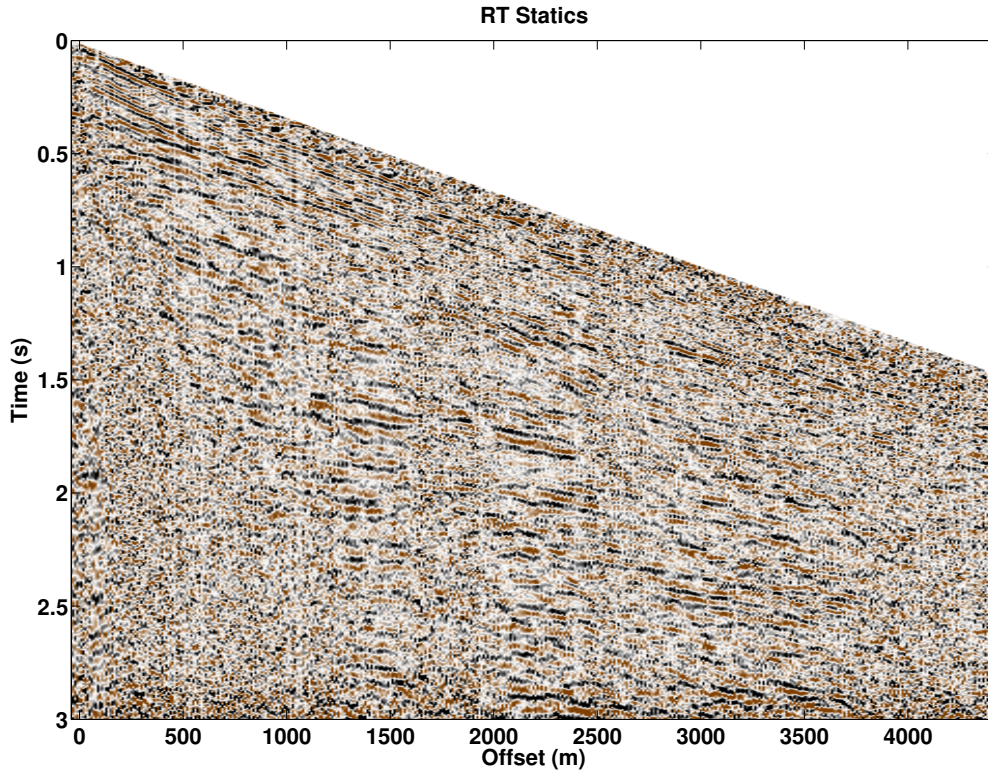
RT Statics

FIG. 14. Radial shot gather after PS-static corrections in the RT domain.

1.6s and improved continuity in the near offset for shallow events. On the other hand, the gather processed in the τ-p domain (Figure 16) displays better coherency on the event at 1.6s and for the large offsets of the shallower events.

Figure 17 show the ACP stack before static corrections. From figure 18 to 20 the stacks after static corrections are shown. One more time the solution in the RT and Snell trace domain are very comparable. Both show important improvements in the shallow events and better resolution at the events below 1.5s. All the false structures displayed on the raw stack were removed and the data now shows a very flat and coherent character.

Finally 20 shows the ACP stack after removing the statics in the τ-p domain. This stack shows better coherency and comparable resolution to the previous two. Below 1.5s the improvement in coherence is very evident. The events between 2s and 2.5s can be tracked for a larger distance. On the other hand, the events above 0.5s are dimmer than in the previous solutions. This agrees with the observations made in the gather were not significant improvement was seen in the short offsets of the shallow events.

The improvement in the coherence of the events may be caused by the filtering effect of the τ-p transform. Since a finite range of p values must be used in the transformation all other p values outside that range are automatically filtered out.
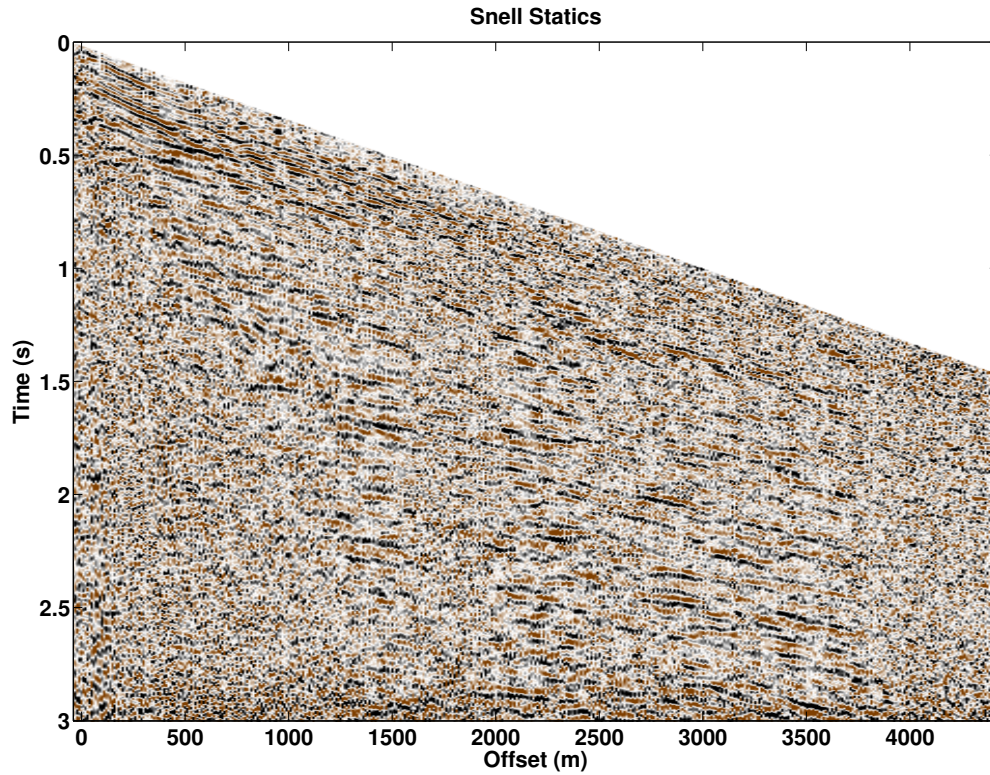
Snell Statics

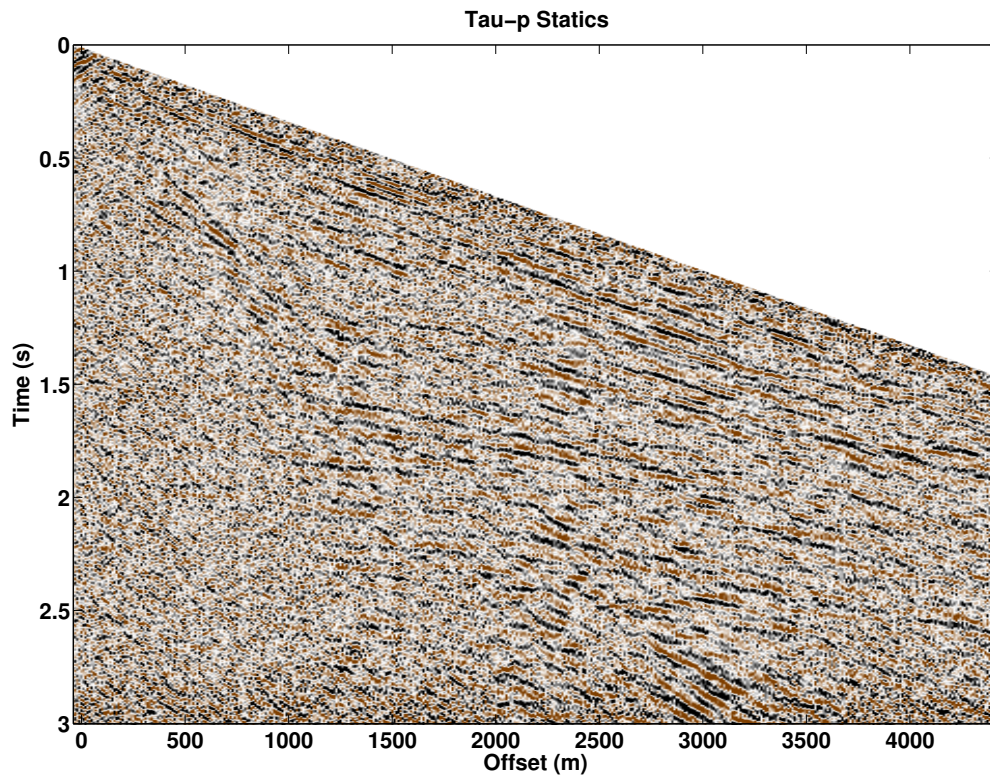FIG. 15. Radial shot gather after PS-static corrections in the Snell rays domain.

Tau–p Statics

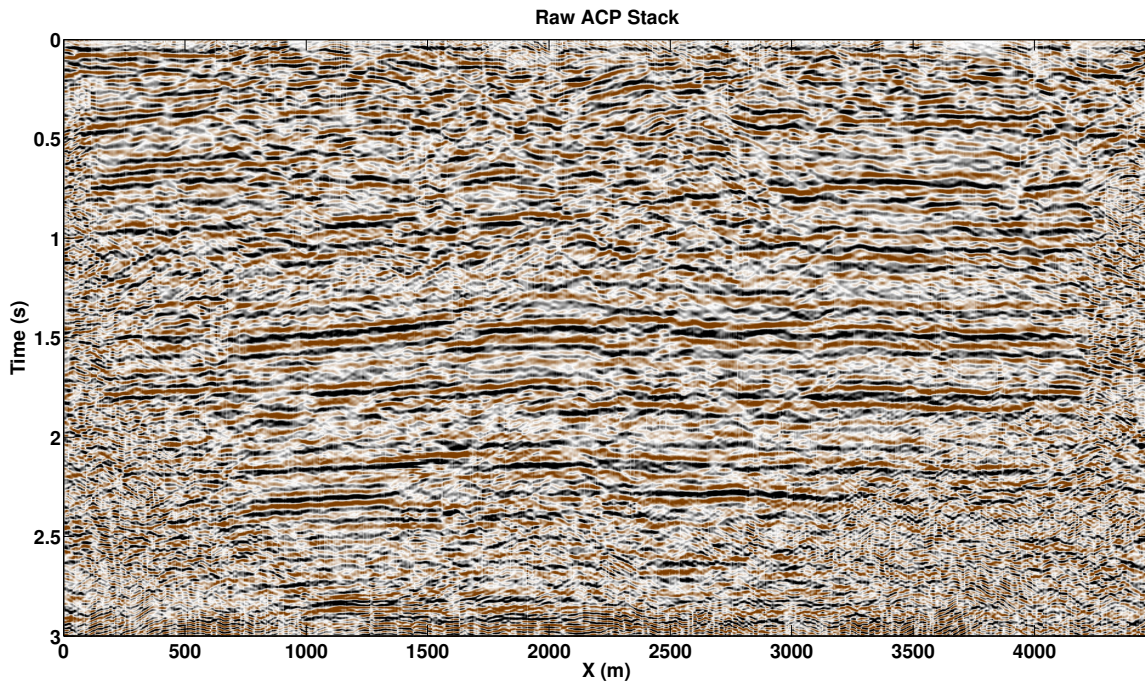FIG. 16. Radial shot gather after PS-static corrections in the τ-p domain.

Raw ACP Stack

FIG. 17. ACP stack before static corrections.

RT Statics ACP Stack
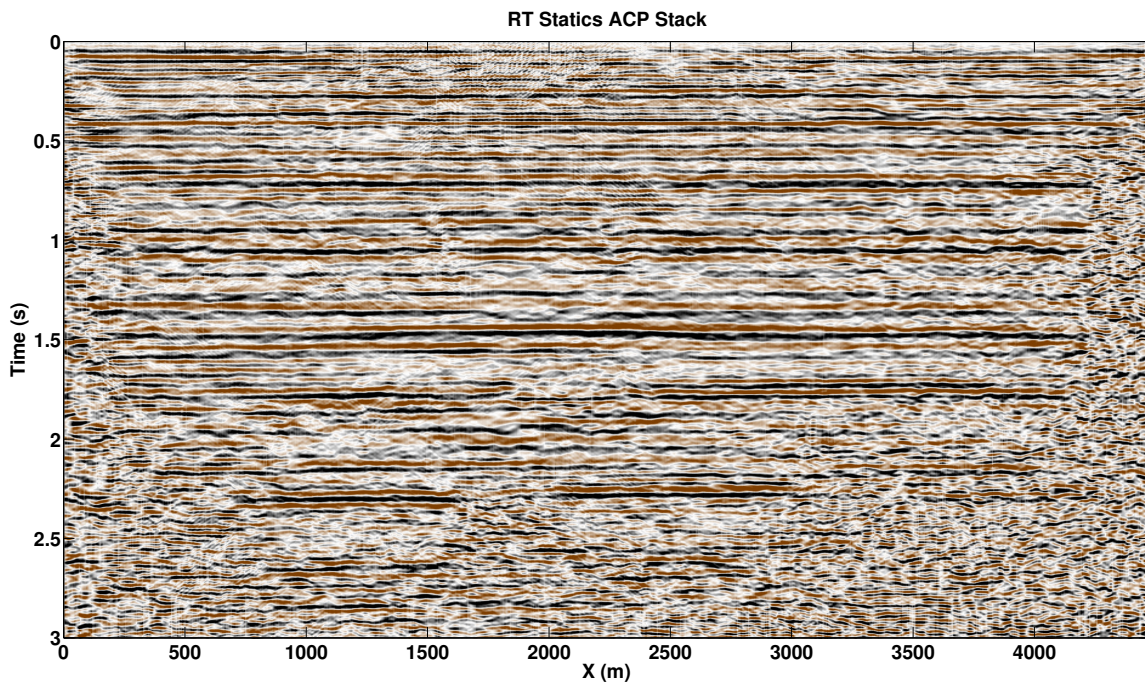
FIG. 18. ACP stack after static corrections in the RT domain.

Snell Statics ACP Stack
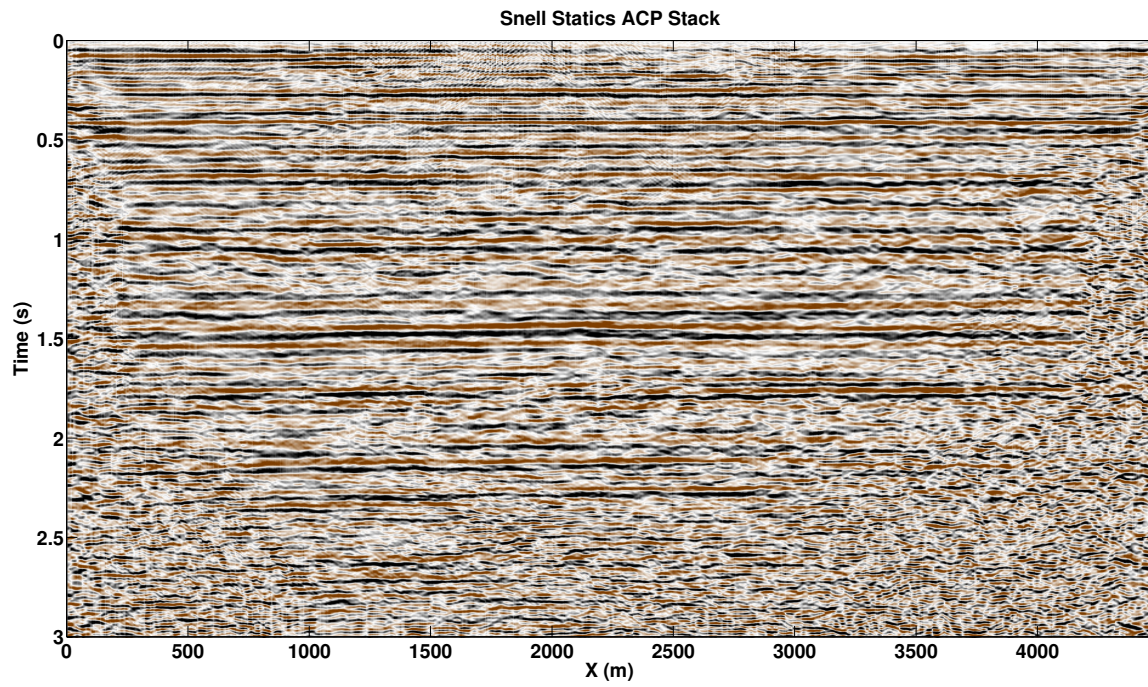
FIG. 19. ACP stack after static corrections in the Snell trace domain.
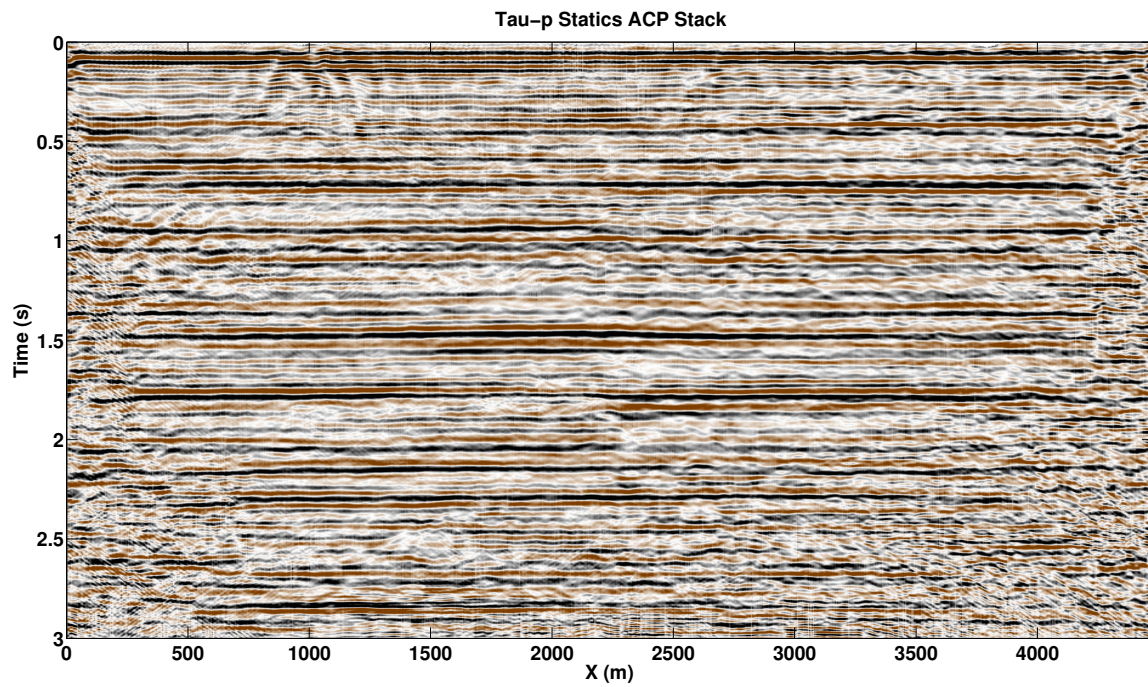
Tau–p Statics ACP Stack

FIG. 20. ACP stack after static corrections in the τ-p domain.

CONCLUSIONS

The solution of the shear-wave static problem in a raypath-consistent framework provides important improvements in coherency and resolution on the stacked sections. The three different transforms compared here successfully achieved the goal of removing the reflection distortions caused by the near surface. However, better coherency for medium and deep events was provided by the solution in the τ-p domain.

The most important problem with the τ-p transformation resides in its invertibility. Due to the band-limited character and finite aperture of the data the inverse transform from the τ-p to the x-t domain loses resolution. For this reason the use of a high resolution τ-p transformation must be tested in future work.

ACKNOWLEDGEMENTS

REFERENCES

Chapman, C. H., 1978, A new method for computing synthetic seismograms: Geophysical Journal of the Royal Astronomical Society, **54**, No. 3, 481–518.

Claerbout, J. F., 1975, Slant-stacks and radial traces: Stanford Expl. Project Report, **SEP-5**, 1–12.

Claerbout, J. F., 1985, Imaging the earth's interior: Stanford Expl. Project Report, 216–219.

Cova, R., Henley, D., and Innanen, K., 2013, Non-stationary shear wave statics in the radial trace domain: CREWES Research Report, **25**, 1–14.

Henley, D., 2000, More radial trace domain applications: CREWES Research Report, **12**, 21.1–21.14.

Henley, D., 2012, Interferometric application of static corrections: Geophysics, **77**, No. 1, Q1–Q13.

Henley, D., 2014, Static corrections via raypath interferometry: recent field experience: Geoconvention 2014, CSEG, Expanded abstracts, in press.

Margrave, G. F., Mewhort, L., Phillips, T., Hall, M., Bertram, M. B., Lawton, D. C., Innanen, K., Hall, K. W., and Bertram, K., 2011, The hussar low-frequency experiment: CREWES Research Report, **23**.

Ottolini, R., 1982, Migration of reflection seismic data in angle-midpoint coordinates: Ph.D. thesis, Stanford University.

Schuster, G., 2009, Seismic interferometry: Cambridge University Press.

Stoffa, P. L., 1989, Tau-p: A plane wave approach to the analysis of seismic data: Kluwer Academic Publishers.

Tatham, R., 1989, Tau-p filtering, *in* Stoffa, P., Ed., Tau-p: a plane wave approach to the analysis of seismic data, Springer Netherlands, **8**, 35–70.